



Influence of freezing directions on ice lens formations in soils

K. Niggemann¹ · M. Ziegler² · R. Fuentes¹

Received: 29 August 2022 / Accepted: 9 January 2024
© The Author(s) 2024

Abstract

This research work presents a comprehensive experimental study of frost heave in a fine-grained material to investigate the effects of top freezing (TF) and bottom freezing (BF) mechanisms with ice lens formation. A novel test device was built to investigate artificial ground freezing (AGF)-related temperature and load boundary conditions. This paper includes 62 frost heave experiments and test observations up to 10 days. The long test duration allows a precise examination of ice lens growth during thermal steady state when the frost line remains largely stable and the ice lens grows. This state corresponds to the holding phase of a practical in situ AGF implementation where the cooling is used to maintain the frozen body thickness. The freezing observations show that BF heaving is larger than TF heaving in most cases. This is caused by the more favorable hydraulic conditions caused by gravitational effects and vertical cracking that occurs during ice lens formation due to suction. This facilitates water accumulation at the ice lens. An applied load reduces the differences between BF and TF conditions beyond a certain value which corresponds to an overburden capable of preventing the formation of the longitudinal cracks.

Keywords Artificial ground freezing · Bottom freezing · Experimental study · Frost heave · Ice lenses · Top freezing

1 Introduction

The method of artificial ground freezing (AGF) was adapted to Civil Engineering works from the mining industry, after the engineer Herman Poetsch invented it in 1883 [1]. The application of AGF to support unstable soils and systems became a very popular method in the last decades, especially for the development of underground infrastructure in inner-city areas. It is an efficient method with a double temporary soil supporting and waterproofing function. However, freezing is also associated to frost-induced soil deformations and frost heave that can cause damage to pipelines, pavements as well as foundations and buildings.

The pore water volume expands by 9% approximately during freezing [2]. Depending on the saturation degree and the hydraulic conductivity, a part of the water can be drained off during freezing. However, in more frost sensitive soils, like silt or clay, the water cannot be expelled during rapid cooling and freezes in situ due to their small hydraulic conductivity. Moreover, pure ice layers (ice lenses) can form in these fine-grained soils which can grow to several centimeters in height depending on the boundary conditions. As water is, by definition, available in soils where AGF is applied, this source of water supports ice lens formation.

One of the first ice lens observations was done by Taber [3, 4]. His freezing studies in different soils pointed out that not only capillary forces pull the water to the ice lens but also thin water films between the solid ice and the grains under high tension led to water movement during freezing. He showed that water migrates from warmer to colder regions and accumulates in thick ice layers, leading to enormous heaving. Ruckli [5] described that ice and the soil grains are enclosed by an adsorption film, with the highest density at the surface of the solid soil grain. The film thickness depends on the load pressure, so increasing load leads to a decreasing film thickness. The presence of the adsorption film was confirmed experimentally by Wilen and

✉ K. Niggemann
niggemann@gut.rwth-aachen.de

M. Ziegler
ziegler@zai-ingenieure.de

R. Fuentes
raul.fuentes@gut.rwth-aachen.de

¹ Institute of Geomechanics and Underground Technology,
RWTH Aachen University, Aachen, Germany

² Ziegler und Aulbach Ingenieurgesellschaft GmbH (Formerly
RWTH Aachen University), Aachen, Germany

Dash [6] by studying the liquid flow in a surface-melted layer of ice. Martin [7] introduced a theory of rhythmic ice banding under unsteady heat flow conditions. The ice crystals grow by water transport from adjacent soil. With decreasing permeability in the unfrozen zone, ice lens growth stops, and a new ice lens forms when the nucleation temperature is reached at another level. Ice nucleation begins at a temperature lower than the temperature at which ice crystals grow significantly (frost line). The freezing point depression is primarily affected by capillarity, adsorption and dissolved salts in the soil water [8–10]. The area between ice lens and frost line is called frozen fringe which contains unfrozen water films around the soil particles and ice in thermodynamic equilibrium [11–19]. Once an ice lens is formed, water from the unfrozen region is drawn into the frozen fringe to maintain the film thickness or thermodynamic equilibrium. The largest ice lens forms when the frost line stops moving because water can be drawn without thermal restriction. This lens is referred to as the decisive ice lens in connection to its greater thickness. Since thermal processes are still occurring during ice lens formation, this phase is also called the quasi-steady state [20].

The thickness of the ice lenses depends on the particle size [21, 22], pore size [23, 24], water availability [25, 26], cooling rate [22, 27, 28] and surface load [4, 10, 29, 30].

In very fine soils, cracking was observed during freezing due to shrinkage processes near the ice lens [31–34]. Vertical cracks arise near the ice lens in the frozen fringe which are linked together, forming columns with a polygonal cross section. These formed polygons lead to an increase in density and permeability. In difference to horizontal ice lenses, the vertical cracks do not significantly change their thickness with time. Even if the small cracks are ice-filled in the frozen fringe, they lead to better water flow to the ice lens via thin water films.

The initiation of ice lenses can be described by temperature [12] or stress conditions [15, 35]. Konrad and Morgenstern [12] introduced a segregation temperature where a new ice lens starts to form. The temperature-dependent critical permeability prevents further water migration toward the frozen soil. O'Neill and Miller [15, 35] introduced the secondary frost heave model. Ice lens initiation occurs by a pressure-dependent approach, when the sum of water and ice pressure in the frozen fringe equals the overburden pressure. These concepts, in their origin or adjusted form, are widely used to explain and predict frost heave with ice lens formation, e.g., [16, 36–42]. A newer concept to define the beginning of ice lens formation is formulated by Style et al. [43] declaring ice lens initiation where supercooling reaches maximum. Zhou and Li [44] using a concept of a separating void ratio, e.g., applied by Sweidan et al. [45]. The separating void ratio is equal to

the void ratio in its most uncompacted status and enables pore ice to connect.

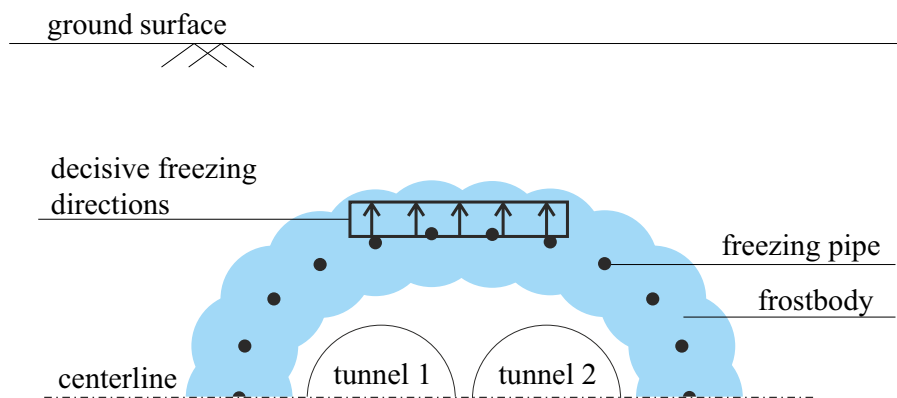
During ice lens formation with water migration and accumulation, hydrothermal properties and the microstructure changes continuously which causes complex mass and energy transfer [46]. Frost heave models have been used to simulate processes of ice lens formation. Ji et al. [47] classified numerical models into the mechanistic frost heave model and the physical field models. The mechanistic frost heave model explains the mechanism of frost heaving and the initiation of discrete ice lenses within the frozen fringe. These models consider the interfacial pressure between water and solid which causes freezing suction [13, 15, 37, 47–51]. Physical field models focus on the moisture, mechanical and temperature field prediction. Freezing expansion is considered by an increasing finite volume of the soil [45, 52–55]. Analytical solutions of frost heave calculation were proposed by Cai et al. [56, 57], using the stochastic medium theory for heave calculation, and by Niggemann et al. [58], using a semi-analytical approach to achieve properties of the frozen fringe for a multifaceted application.

AGF and natural soil freezing in fine material present similar soil freezing mechanisms, including the formation of ice lenses. However, the different boundary conditions present in both scenarios on the total heave and ice lens formation have not been fully presented to date. The freezing direction is of interest and shows different characteristics as explained in the next section and observed from the literature presented in Table 1. In AGF, freezing occurs in multiple directions (e.g., tunnel cross section), where the largest surface heave occurs due to upward freezing (Fig. 1) using brine at temperatures of ≈ -35 °C [59]. Considering seasonally soil freezing in natural conditions, the frost penetrates the soil from the top downward due to subzero temperatures, a condition that may also apply to AGF, but usually at temperatures above -15 °C [60]. The different temperatures are important as larger temperature gradients are known to reduce ice lens formation during frost penetration.

At natural freezing, the investigations focus on frost heave during ongoing frost penetration. In that case the frost line, where ice lenses form, is a moving boundary and the ice lens formation is restricted by the freezing velocity. An apparently infinite ice lens can form when the frost line maintains at a specific position due to thermal (quasi-) equilibrium. (There are still thermal processes due to ice lens formation, but of minor interest concerning frost penetration.) This quasi-steady state is comparable with the holding phase at AGF, where the thickness of the frozen body is only preserved but over a longer time period. Assuming infinite ice lens growth, the quasi-steady state at the AGF is the governing state to be considered.

Table 1 Frost heave test conditions from the literature

| | Specimen size [cm] | Soil type | Freezing direction | Freezing temperature/-conditions | Load [kPa] |
|-----------------------------|---|--|--------------------|--|--|
| Kaplar [61] | $h=15.2$ $d_{\text{top}}=14.6$ $d_{\text{bottom}}=14.0$ | Gravelly silty sand | TF | Near 0 °C; Frost Penetration: 0.6–1.3 cm/d | 3.4 |
| Penner and Ueda [62] | $h=10.2$ $d=10.2$ | Silty sand, sandy silt, clayey silt | BF | up to –2 °C | consol.: 392–490 freezing test: 49–490 |
| Loch and Kay [8] | $h=7.0\text{--}7.4$ $d=3.7$ | New Hampshire Silt | BF | up to –7 °C | 7.7–65.2 |
| Konrad and Morgenstern [12] | $h=25.0$ $d=10.0$ | Devon Silt | TF | –2.5 to –6.2 °C | consol.: 210 |
| Konrad and Morgenstern [64] | | | TF | –3.5 to –6.0 °C | freezing test: – |
| Konrad and Morgenstern [65] | | | BF | $\text{grad}T_f=$ 0.63–1.11 °C/cm | consol.: 210 freezing test: 45–400 |
| Jin et al. [63] | $h=10.0$ $d=10.0$ | Joomunjin Sand and Kaolinite, weathered granite | BF | –8 to –9.5 °C | 1.62 |

**Fig. 1** Freezing directions at AGF of a tunnel cross section

In the last decades, many frost heave tests were carried out by several researchers who investigated the frost sensitivity of different soils as well as the influences of freezing temperatures and/or loads on frost heave, e.g., [12, 27, 61–65]. Table 1 summarizes the test conditions. The dimensions of the test cylinders vary in height h between 7 and 25 cm and in diameter d between 3.7 and 14.6 cm. Kaplar [61] used a conical test cylinder to reduce friction between the specimen and the cylinder during frost heaving while

freezing the sample from the top downward (top freezing—TF). Others have used freezing conditions from the bottom upward to reduce friction (bottom freezing—BF).

The literature shows frost heave observations using different freezing directions to improve the technical implementation (cf. Table 1), frost heave tests and models considering multidirectional freezing [66, 67], or permeability investigations due to direction dependent freeze–thaw cycles [68]. But a systematic study to compare the

heave development of the two main freezing directions associated to natural and artificial freezing is missing. Experimental frost heave studies are usually conducted with standard test devices investigating one freezing direction. Therefore, this study focuses on the frost heave development using a test device which allows a simultaneous investigation of two samples, one freezes from the top, the other from the bottom. This enables a direct comparison of heaving under identical thermal or load conditions.

Hence, we quantify heave differences for top-down freezing (TF) and bottom-up (BF) freezing in terms of AGF-related boundaries concerning thermal and load conditions, which are different to natural soil freezing conditions. We carried out 62 frost heave experiments in a novel frost heave apparatus to ensure identical boundary conditions. In comparison to common frost heave tests, a long test duration of 10 days was selected because it is necessary to investigate the thermal steady state in which the largest ice lens is formed. These observations are also novel, especially in combination with different boundary conditions.

For this purpose, basics on the experimental design, the instrumentation, the test material and the testing program are given in Sect. 2. The following Sect. 3 explains the test evaluation, which includes necessary information for the result analysis in Sect. 4. Finally, the results are briefly summarized, and conclusions are given in Sect. 5.

2 Experimental design and test description

2.1 Setup

The new experimental setup is shown in Fig. 2, and detailed descriptions of specific elements and instrumentation are given in Table 2. The dimensions of the cylindrical specimen are 25 cm in diameter and 20 cm in height. The test cylinder consists of eight PVC ring elements, with a thickness of 2.5 cm, connected by a tongue and groove system to prevent lateral displacement. The ring elements lying on top of each other were sealed by a rubber ring so that no water leaks out of the unfrozen soil. For specimen installation, the rings were additionally screwed together. During the freezing test, the ring elements can be pulled and move apart vertically, so that the soil samples do not undergo any frictional resistance due to the vertical expansion. The top and the bottom of the samples, respectively, were cooled by a freezing element ①. The freezing temperature was controlled by a temperature sensor placed in the freezing element. A water reservoir ② was connected to a filter plate ③ at the warm side of the sample, providing a constant water supply under atmospheric pressure for ice lens formation. In the BF tests, the position of

the water reservoir placed at the top of the sample was adjusted during the freezing test to compensate for the vertical specimen expansion. The warm end of the soil sample was additionally heated by a heating plate ④ to avoid freezing of the overall sample. The test cylinders were covered with a Styrodur insulation (BASF, Germany). All tests were carried out in a climatic chamber with a constant temperature of 15 °C (initial temperature of the soil before freezing) and humidity of 40% to exclude influences such as seasonal fluctuations.

For the experimental study without considering overburden pressure (Fig. 2a), a load results only from the apparatus elements (i.e., the porous heating plate for BF and the freezing plate for TF) and an additional static 10 kg load to ensure a frictional connection between the plates and the sample. This results in a total load of $p=3.6$ kPa.

The test series considering overburden load (Fig. 2b) were carried out using a drive ⑤ to apply loads between 50 and 250 kPa to the sample from the top. After consolidation, the soil has settled in the test cylinder. Using an adapter (steel plate) ⑥ that was installed between the soil and the freezing element from the beginning, heat transfer from the freezing element into the soil by conduction was ensured during the whole test procedure. (The freezing element cannot enter the test cylinder due to connections.)

2.2 Instrumentation

For data recording, temperature sensors ⑦ are distributed over the sample height, see Fig. 2 and Table 2. After consolidation, the temperature sensors were placed into the soil sample through small openings in the ring elements. During frost heaving, the sensors move together with the ring elements. The vertical deformation was measured by displacement transducers that are connected to the temperature sensors ⑧. The displacement transducers were attached to the ring elements that move vertically during the freezing process. For the data recording of the total uniaxial deformation at the top of the specimen, the same type of displacement transducer was used ⑨. This temperature and displacement monitoring allows the calculation of the freezing front velocity, which is important to distinguish between the thermal transient and steady state (cf. sub-Sect. 3.2.1). To determine the water inflow into the sample due to suction, the mass of the water supply was recorded by a load cell ⑩. The load of the drive was controlled by a connected load cell ⑪.

2.3 Test material and preparation

The test material was produced artificially to ensure an equal composition for all tests and, thus, to improve the repeatability and consistency of the results. With a liquid

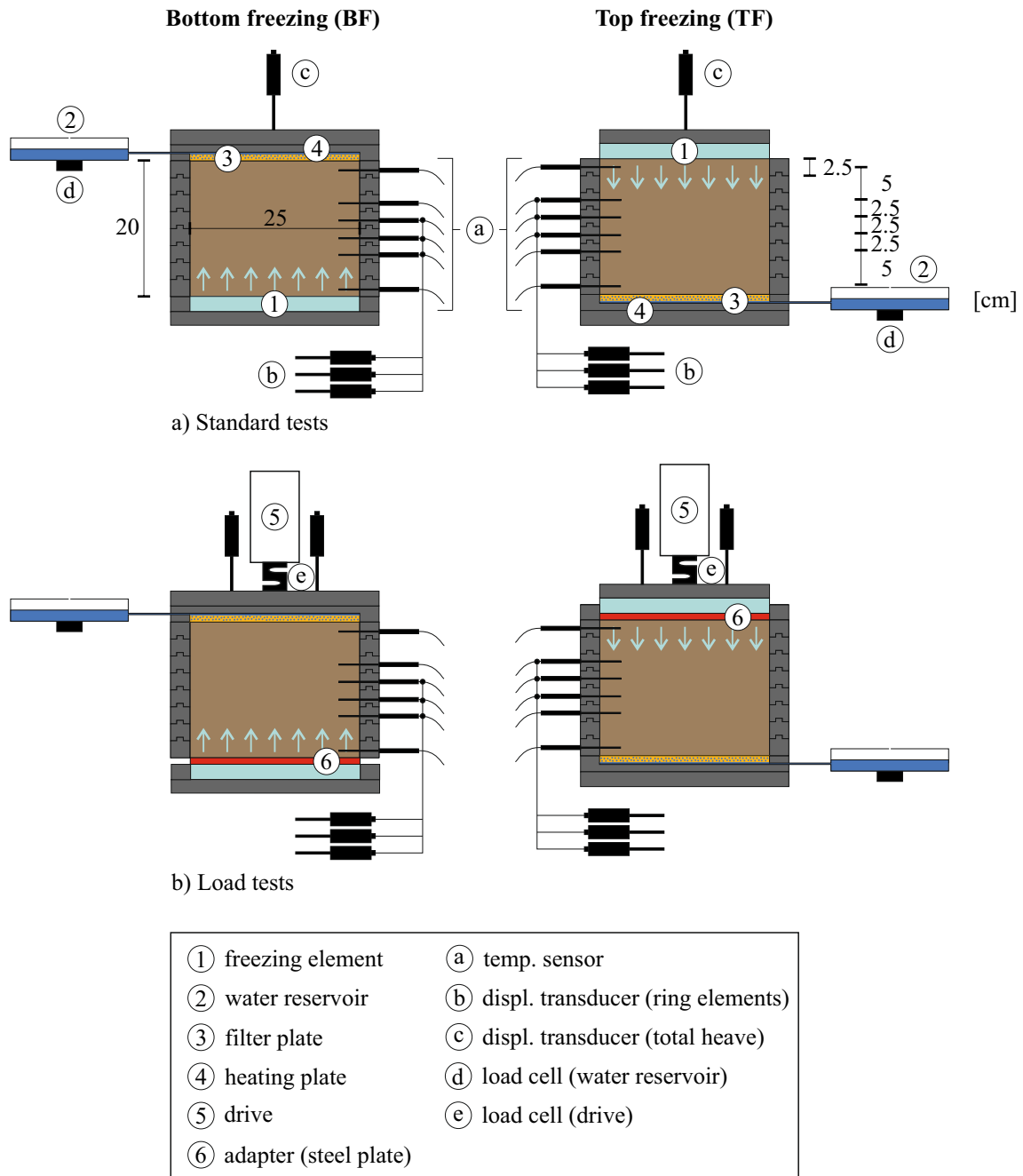


Fig. 2 Test setup for TF and BF, for a standard tests and b load tests

limit (LL) of 32.9% and a plasticity index (PI) of 14.5%, the soil can be classified as a lean clay (CL, Unified Soil Classification System). The grain size distribution can be found in [40]. The dry material was prepared with an initial mass water content of 20% to ensure a high saturation as well as an appropriate consistency, and subsequently stored for 24 h to ensure that the water can penetrate into the pores. Afterward, the initial water content of the soil was proved for each test by a drying procedure where the material is heated up to 105 °C for 4 days to determine the previous

water content in the sample. The values of the initial mean mass water content \bar{x}_w and saturation \bar{x}_{Sr} , and standard deviation σ_w and σ_{Sr} for the 32 TF and 30 BF tests, presented in Table 3, confirm the good repeatability of the process.

The hydraulic conductivity of the soil was tested several times with the same initial conditions of porosity and saturation degree as the test specimen. The mean value is $1.3 \cdot 10^{-10}$ m/s ($\sigma_k = 5.3 \cdot 10^{-11}$ m/s) or $1.8 \cdot 10^{-17}$ m² ($\sigma_K = 7.0 \cdot 10^{-18}$ m²). The soil was compacted in eight layers in the

Table 2 Description of setup elements and instrumentation

| Name | Function | Description |
|---------------------------|---|--|
| ① freezing element | sample cooling | connected to circulation thermostat (CC-508, Huber Kaeltemaschinenbau AG, Germany) refrigerant: silicone oil (Thermodfluid M60.115/200.05, Huber Kaeltemaschinenbau AG, Germany) |
| ② water reservoir | water supply | connected to a filter plate ③ large diameter ($d=29$ cm) o sufficient water availability o very low water head of approx. 1 cm |
| ③ filter plate | water distribution | connected to the heating plate ④ |
| ④ heating plate | sample heating | connected to a warming circulation thermostat (Kiss 104A, Huber Kaeltemaschinenbau AG, Germany) circulating fluid: water |
| ⑤ drive | applying load | load application by cylinder connected to electric spindle (Spindeltrieb 10 kN+SMS 94, Pero, Germany) deformation-controlled loading (0.5 mm/min) until the required load was applied constant load during consolidation and freezing phase automatic load control every 60 s |
| ⑥ steel plate | adapter for load tests | $d=1$ cm (equal in all load tests depending on the pretested settlement after maximum loading with 250 kPa) |
| ① temp. sensors | temperature measurement | MWT1/10, TMH GmbH, Germany measurement precision 1/10 DIN B: $\Delta T = \pm(1/10(0.30^\circ\text{C} + 0.005 \text{ T}))$; $T = \text{temperature } [^\circ\text{C}]$ |
| ① displacement transducer | vertical displacement measurement (ring elements) | LRW2-C-50, WayCon Positionsmesstechnik GmbH, Germany measurement precision: $\pm 0.1\%$ |
| ① displacement transducer | vertical displacement measurement (total heave) | LRW2-C-50, WayCon Positionsmesstechnik GmbH, Germany measurement precision: $\pm 0.1\%$ |
| ① load cell | load measurement (water reservoir) | for calculation of the water intake into the soil sample S2, HBM, Austria measurement precision: $\pm 0.02\%$ |

Table 2 (continued)

| Name | Function | Description |
|-------------|--------------------------|--|
| ① load cell | load measurement (drive) | load control of the drive KDB, Pero, Germany measurement precision: $\pm 0.02\%$ |

Table 3 Mean value \bar{x} and standard deviation σ of initial water content w and saturation S_r for TF and BF

| | $n[-]$ | $\bar{x}_w[\%]$ | $\sigma_w[\%]$ | $\bar{x}_{S_r}[\%]$ | $\sigma_{S_r}[\%]$ |
|----|--------|-----------------|----------------|---------------------|--------------------|
| TF | 32 | 20.37 | 0.55 | 91.70 | 2.60 |
| BF | 30 | 20.33 | 0.60 | 91.30 | 2.73 |

test cylinder by 40 blows with a 4.5 kg proctor hammer. The mean moist density achieved is 2.022 g/cm^3 ($\sigma_\rho = 0.017 \text{ g/cm}^3$).

The prepared soil in the test cell was stored for approx. 24 h in the climatic chamber at 15°C to ensure a uniform material temperature at the beginning of each test. The material temperature was monitored by the temperature sensors already installed. After acclimatization, when all sensors reached 15°C , the freezing process started. Simultaneously, the tempering process began on the warm side of the specimen. Depending on the thermal boundary conditions, one freezing test took up to 2 days to reach thermal quasi-steady state conditions. Afterward, the test ran about 8 more days to provide a long thermal steady state phase.

2.4 Testing program

The main task of the experimental program is the observation of TF versus BF under variation of the following parameters:

- absolute freezing temperature T_f
- temperature gradient in the frozen area $gradT_f$
- external load p

Additionally, a test was carried out with *restricted water supply* W_{ws0} at a freezing temperature of $T_f = -10^\circ\text{C}$ to study the effect of no additional available water.

Table 4 summarizes the main values of the tests. The parameter $T_{c,ts}$ describes the recorded cold side temperature during steady-state conditions measured by the nearest temperature sensor to the cold edge (cf. Fig. 2). Similarly, $T_{w,ts}$ describes the measured temperature on the warm side. A fully water supply by the external reservoir is given by

Table 4 Main values of the experimental parameter study

| Tested parameter | T_f [$^{\circ}\text{C}$] | $T_{c,ts}$ [$^{\circ}\text{C}$] | $T_{w,ts}$ [$^{\circ}\text{C}$] | W_{ws} [%] | $gradT_f$ [$^{\circ}\text{C}/\text{cm}$] | p [kPa] | n_{TF} [-] | n_{BF} [-] |
|----------------------------------|------------------------------|-----------------------------------|-----------------------------------|--------------|--|----------------------|--------------|--------------|
| T_f [$^{\circ}\text{C}$] | -5 | -4.3 | 10.4 | 100 | 1.0 | 0 | 3 | 3 |
| | -7.5 | -6.9 | 8.6 | | | | 2 | 2 |
| | -10 | -9.0 | 8.0 | | | | 6 | 4 |
| | -12.5 | -11.3 | 6.9 | | | | 1 | 1 |
| | -15 | -13.9 | 5.4 | | | | 4 | 4 |
| | -17.5 | -16.0 | 4.6 | | | | 1 | 1 |
| W_{ws0} [-] | -10 | -9.2 | 6.9 | 0 | 1.0 | 0 | 1 | 1 |
| $gradT_f$ [$^{\circ}\text{C}$] | -15 | -13.5 | 13.6 | 100 | 1.5 | 0 | 3 | 3 |
| | -7 | -6.5 | 5.2 | | 0.8 | | 3 | 3 |
| p^* [kPa] | -12.5 | -12.2 | 6.0 | 100 | 1.0 | 50 | 1 | 1 |
| | | -12.2 | 5.5 | | | 100 | 1 | 1 |
| | | -12.4 [†] | 5.2 | | | 150 | 1 | 1 |
| | | -12.4 [†] | 4.7 | | | 200 | 1 | 1 |
| | -5 | -12.5 [†] | 5.0 | | | 250 | 1 | 1 |
| | | -4.9 | 9.8 | | | 50 | 1 | 1 |
| | | -5.0 [†] | 9.2 | | | 250 | 1 | 1 |
| | | -9.6 [†] | 6.7 | | | 250 | 1 | 1 |

*placement of temperature sensors after consolidation

[†]extrapolated values on cold side; due to consolidation the nearest cold side temperature sensor could not be placed

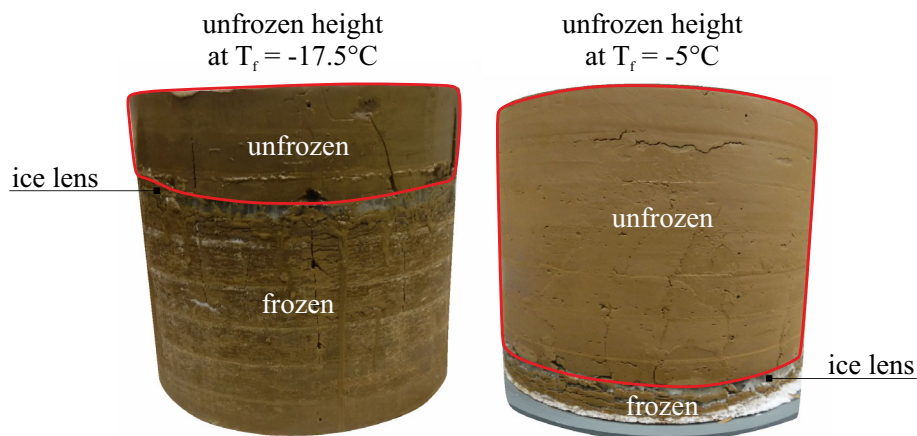


Fig. 3 Unfrozen soil part/flow path (red box) for a freezing temperature of -17.5 $^{\circ}\text{C}$ (left) and -5 $^{\circ}\text{C}$ (right), BF (color figure online)

$W_{ws} = 100\%$, whereas $W_{ws} = 0\%$ means no water supply from the reservoir. The values for n_{TF} and n_{BF} correspond to the number of experiments for one parameter variation. Where more than one test was performed, the figures are mean values for that single parameter combination.

The absolute freezing temperature T_f controls the frost penetration as show in Fig. 3 for a BF test. Values of T_f between -5 and -17.5 $^{\circ}\text{C}$ were imposed using a temperature sensor placed in the freezing element as control. On the warm side, the water is heated up to 25 $^{\circ}\text{C}$ that prevents

freezing of the whole sample. (Please note the actual temperature of the warm side is lower than 25 $^{\circ}\text{C}$ due to the higher cooling capacity in the system.) The temperature gradients along the frozen or unfrozen soil remain constant after reaching thermal quasi-steady state conditions.

To investigate the influence of different temperature gradients $gradT_f$ in the frozen area on frost heave and ice lens formation, the cold and warm side temperatures were adjusted to reach the same frost penetration depth (in the center of the sample) at different freezing and heating

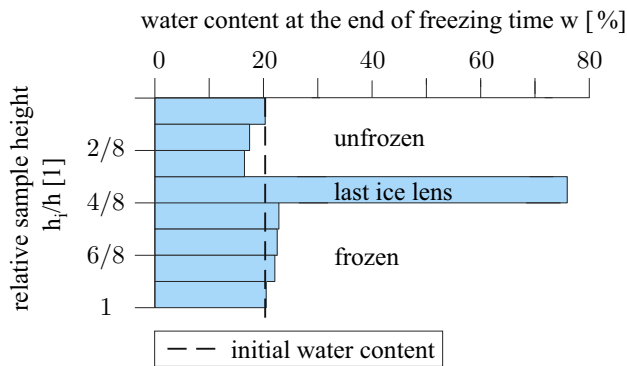


Fig. 4 Soil water distribution after freezing ($T_f = -10$ °C) for BF

temperatures. The resulting temperature gradients are 0.8 °C/cm, 1.0 °C/cm and 1.5 °C/cm (see Table 4).

For the tests with *external load* p , the soil samples were loaded between 50 and 250 kPa, 50 kPa intervals, from the top of the sample, corresponding to overburdens of approximately 2.6 m, 5.3 m, 7.9 m, 10.5 m and 13.2 m ($\rho_{\text{soil}} \approx 1.9$ g/cm³).

3 Evaluation of experimental tests

3.1 Sample examination at the end of the freezing test

After each test, the sample was removed from the test cylinder and visually observed. Subsequently, the sample water content w was determined in the longitudinal direction by drying procedure (cf. subsection 2.3). For this purpose, the sample (total height h) was divided into 8 layers with a thickness of approx. $h_i \approx 2.5$ cm. (The final ice lens thickness was between ≈ 0.5 cm and ≈ 1.5 cm.) The results provide details about the water distribution in the soil sample after freezing. Figure 4 shows the water distribution at the end of BF with a freezing temperature of -10 °C as an example. (Others are provided in the Supplementary Material 1 and 2) With different freezing temperatures the position of the ice lens changes, but qualitatively the water distribution in the frozen and unfrozen part is very similar. In the frozen area, the water content slightly increases due to minor ice lens formation during transient freezing. In the unfrozen area close to the last ice lens, which is built under quasi-steady state conditions, the water content decreases. It indicates that soil water was drained off the area near the ice lens without a direct flow from the reservoir water through suction [69].

This effect is clarified by Fig. 5, which shows the measured reservoir water mass that is sucked into the soil sample as a proportion of the total water mass that is used for the ice lens formation. The dashed line indicates the pore

water mass used for ice lens formation, calculated as the difference between the measured sucked water from the reservoir and the total water mass for ice lens formation. The latter is calculated as the ice lens heave (heave measurement) divided by the expansion factor of 1.09 due to phase change. At the beginning of ice lens formation, most of the sucked water comes from water-filled soil pores, because the water from the external reservoir is initially saturating air-filled pores before reaching an unrestricted flow to the ice lens. With time, most water for ice lens formation comes from the reservoir, but the initial water content at the growing ice lens cannot be restored, resulting in a final soil water distribution as shown in Fig. 4. The water near the growing ice lens drains off without sufficient water supply and a pattern cross section with openings growing along the unfrozen sample height is formed (Fig. 6).

The cracks were investigated after each freezing process (Fig. 6). This phenomenon of crack formation was also observed by other scientists, e.g., [31, 33] and [70], and it applies particularly to impermeable soils where greater suctions occur. The crack formation increases the water migration to the ice lens [34, 45, 71, 72].

The lower the freezing temperature the shorter it takes for the water from the reservoir to reach the ice lens and become dominant. With lower freezing temperatures and, therefore, a shorter unfrozen height or flow path, increasingly reservoir water is used for ice lens formation. The shorter flow path of the external water to the ice lens influences the hydraulic gradient, which is calculated by the pressure difference between ice lens and water reservoir and the flow path. Figure 5 shows that for BF, the supply of reservoir water is improved in comparison to TF which can be explained by longitudinal cracks along the unfrozen sample height that enhance the water supply by gravity at BF.

3.2 Evaluation of measured data

3.2.1 Determination of 0 °C isotherm

Figure 7 shows the recorded temperature and position over time for each temperature sensor used to calculate the moving frost line, or 0 °C isotherm. (Sensor positions are given in Fig. 2.)

This is important to calculate the temperature gradients in the frozen and unfrozen soil. The temperature distribution is also necessary for the definition of the thermal transient and quasi-steady states. Since the measured isotherms around 0 °C almost run parallel (cf. Fig. 7), the course of the 0 °C isotherm was used to define the onset of the quasi-steady state and, therefore, the ice lens formation. Figure 8 shows a calculated 0 °C isotherm position (a) and the corresponding

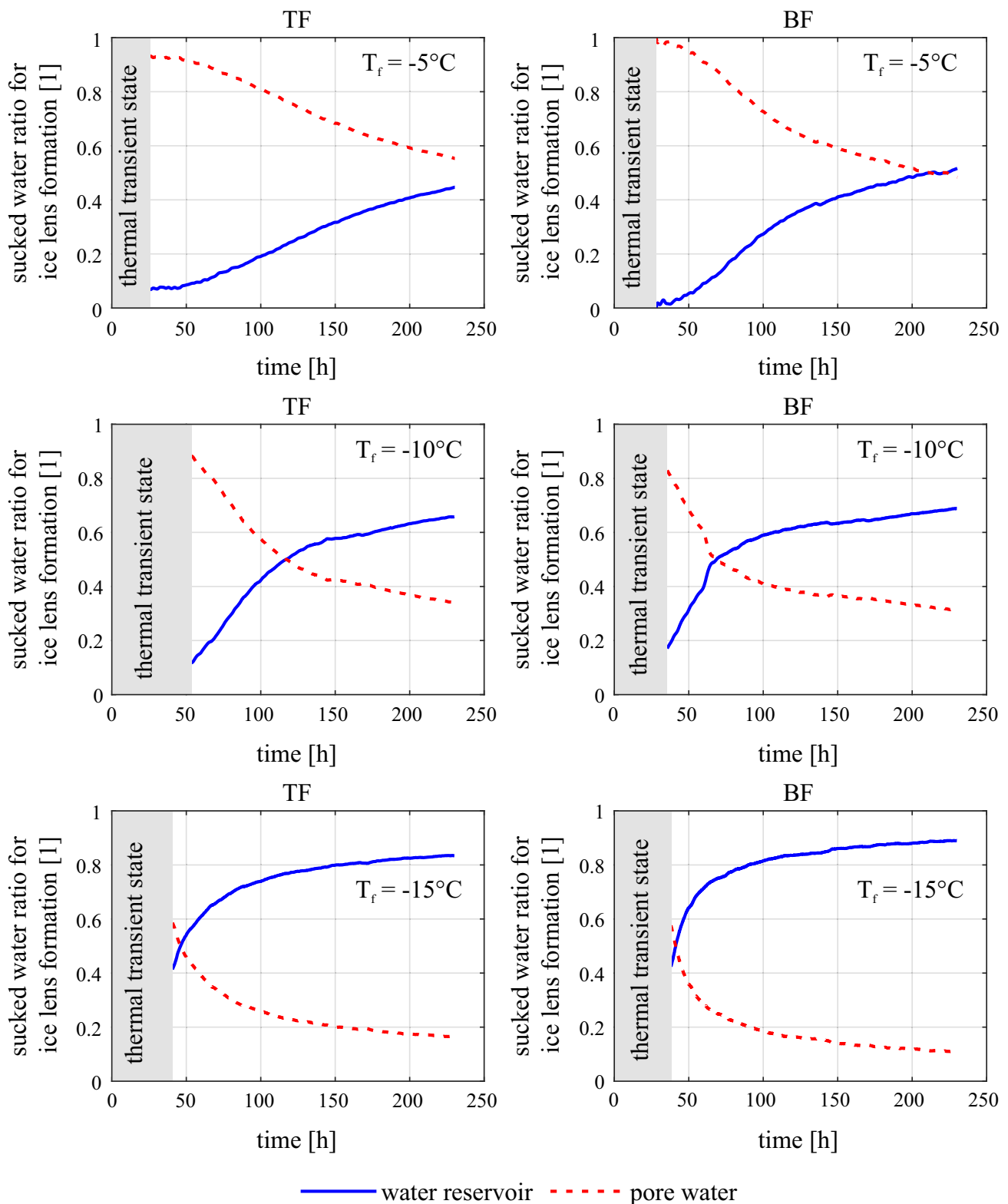


Fig. 5 Origin of the water for the formation of ice lenses at different freezing temperatures for TF and BF

frost penetration velocity v_{fp} (b). Figure 8b allows differentiating between the two distinct stages. When reaching thermal quasi-steady-state conditions, the frost penetration

velocity approaches zero. The beginning of the thermal quasi-steady state is also defined by a critical frost penetration velocity $v_{fp,crit}$ less than 0.01 cm/h. From this point

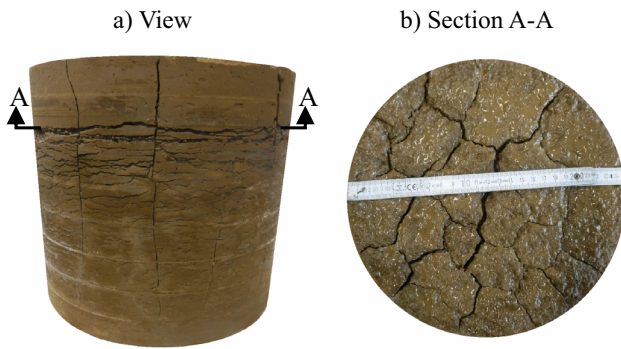


Fig. 6 Longitudinal crack formation of a BF sample

onward only ice lens growth occurs. Similar graphs apply to other temperatures and are presented in the Supplementary Material 3–6.

3.2.2 Determination of the heave proportions

Figure 9 shows the results of frost heave at thermal transient and quasi-steady state for BF at a freezing temperature of

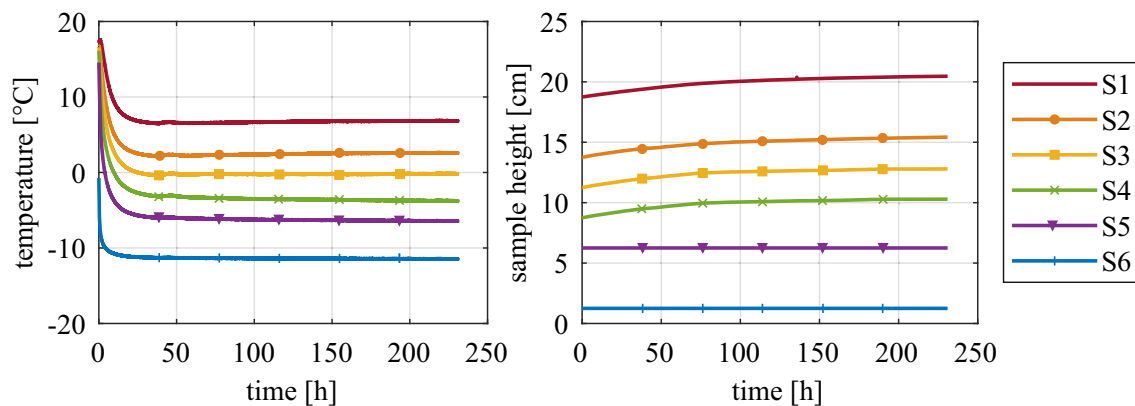


Fig. 7 Recorded temperature and position over time for the temperature sensors (S) for BF with a freezing temperature of $-12.5\text{ }^{\circ}\text{C}$

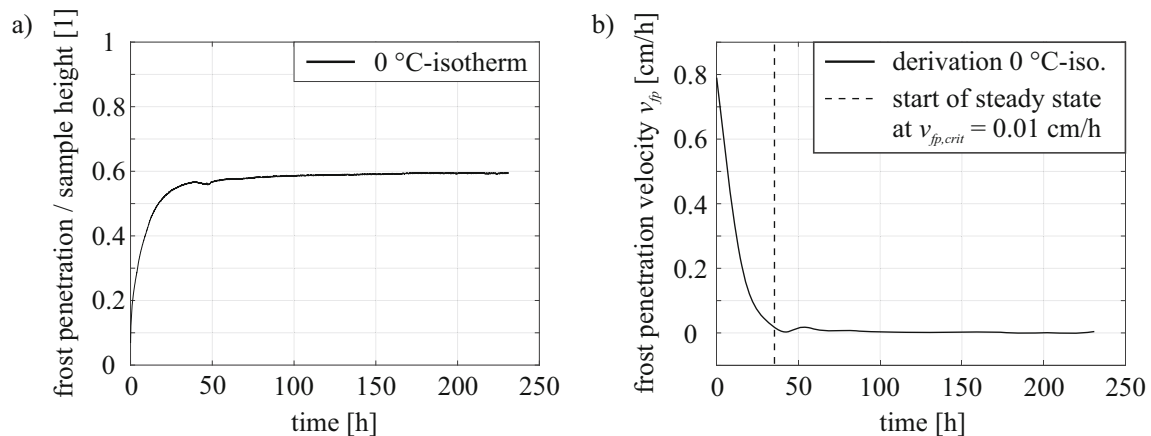


Fig. 8 **a** Course of the $0\text{ }^{\circ}\text{C}$ isotherm and **b** corresponding frost penetration velocity for BF with a freezing temperature of $-12.5\text{ }^{\circ}\text{C}$

$-10\text{ }^{\circ}\text{C}$. The total heave at thermal transient conditions is very low compared to the total heave at the thermal quasi-steady state, showing the importance of the thermal quasi-steady state for AGF. In the thermal transient state, the pore water heave h_{PW} is determined by the one-dimensional pore water expansion of 9% due to the frost penetration $x(t)$ using the porosity n and the saturation degree S_r as shown in Eq. 1. It is assumed that the water freezes at $0\text{ }^{\circ}\text{C}$ and does not expand in air-filled voids.

$$h_{PW}(t) = 0,09 \cdot n \cdot S_r \cdot x(t) \quad (1)$$

The difference between total heave (h_{tot}) and pore water expansion (h_{PW}) is the calculated ice lens heave (h_{IL}). Consolidation effects are neglected because the load on the soil is very low at about 5 kPa, except for load tests. For thermal quasi-steady state, the ice lens heave is equal to the total heave.

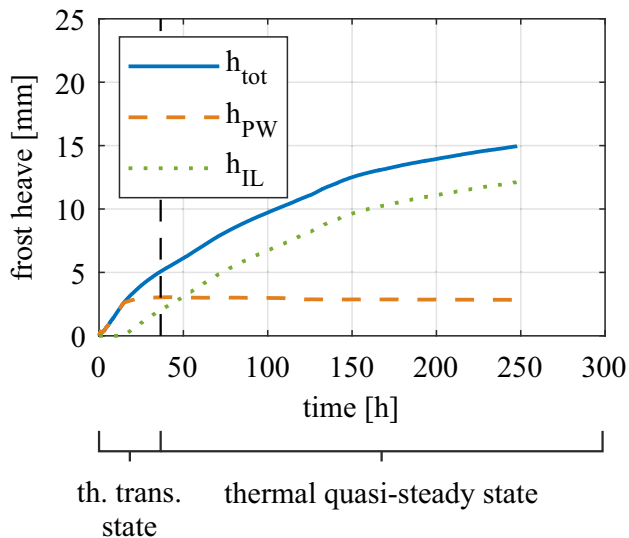


Fig. 9 Frost heave during thermal transient and quasi-steady state for a freezing temperature of $-10\text{ }^{\circ}\text{C}$, BF

4 Test results

The following subsections contain the frost heave results of 62 experiments according to the parameter variations explained in subsection 2.4 and summarized in Table 4.

4.1 Absolute freezing temperature T_f

The actual freezing temperature (T_f) determines the frost penetration depth and therefore the frozen and unfrozen soil height. The lower the freezing temperature the greater the frost penetration or frozen part of the soil at the thermal quasi-steady state. To compare the results during thermal transient freezing, with pore water expansion and minor ice lens formation, the frost heave is related to the frozen part. The relationship between frost heave and the height of the frozen part is proportional because all tests have similar values of volumetric porosity n and saturation degree S_r (cf.

Table 3 and Eq. 1 in subSect. 3.2.2). Figure 10 shows a similar curve for all tests. At TF, the slope of the frost heave related to the frozen height is greater at the beginning, decreases with time and ends up in a straight line that indicates a constant rate of frost heave. At BF, the curve is like TF, except of a lower gradient at the beginning of freezing due to the overburden soil weight which decreases frost heaving.

Generally, ice lenses grow thicker (greater heave) at a decreasing frost penetration rate (i.e., higher freezing temperatures) because more time is available for water accumulation (refer also to Fig. 5).

Of particular interest is that most lines show a similar linear trend toward the end of this transient stage. Table 5 shows a straight line fit to the lines for this latter part, showing that for all temperatures with absolute temperature lower than $-10\text{ }^{\circ}\text{C}$, the frost heave increases at the same rate with time. This agrees with the fact that during this transient stage, the ice lens formation is minimal, and the frost heave is a consequence of porewater expansion, which depends on porosity and the amount of freezing water, which can be estimated as the position of the frost line. However, for higher temperatures, $-5\text{ }^{\circ}\text{C}$ and $-7.5\text{ }^{\circ}\text{C}$, the heave grows faster relative to the frozen height (Table 5, in bold) indicating additional heaving by ice lenses.

The differences between BF and TF are related to the absolute values shown in Fig. 10 where BF shows generally lower values of heave. This shift is possibly due to the increased overburden in BF. Table 5 shows that the actual trends are generally very similar between BF and TF which indicates that, even at transient stage, the frost heave growth rate is governed by the temperature boundary conditions.

Furthermore, the heave result due to a restricted water supply (W_{ws0}) follows the other curves, showing that the restricted water supply does not have an impact on frost heave during transient freezing because of minor ice lens formation.

The heave at thermal quasi-steady-state conditions results only from ice lens formation and is shown in Fig. 11. In general, the lower the temperature, the larger the ice lens heave is. The increasing frost penetration due to the lower temperature boundary condition decreases the flow path between ice lens and water reservoir. A shorter flow path enhances the water supply for ice lens formation due to an increasing water flow velocity from the water reservoir to the ice lens. Therefore, at thermal quasi-steady-state conditions, the frost heave depends on the flow path (unfrozen soil height) and is not controlled by the height of the frozen part (cf. transient state). The frost heave rate due to a restricted water supply (W_{ws0}) strongly decreases over time as only the surrounding soil water can be used to form the ice lens. At this stage, it is therefore critical that water is available for heave to continue.

Table 5 Linear heave slope for transient freezing

| | (Frost heave/frozen height)/time [1/h] | |
|---------------|--|----------------|
| | TF | BF |
| $T_{f,-5}$ | 0,00131 | 0,00139 |
| $T_{f,-7.5}$ | 0,00099 | 0,00118 |
| $T_{f,-10}$ | 0,00077 | 0,00083 |
| $T_{f,-12.5}$ | 0,00083 | 0,00103 |
| $T_{f,-15}$ | 0,00091 | 0,00087 |
| $T_{f,-17.5}$ | 0,00084 | 0,00089 |
| $W_{ws,-10}$ | 0,00075 | 0,00087 |

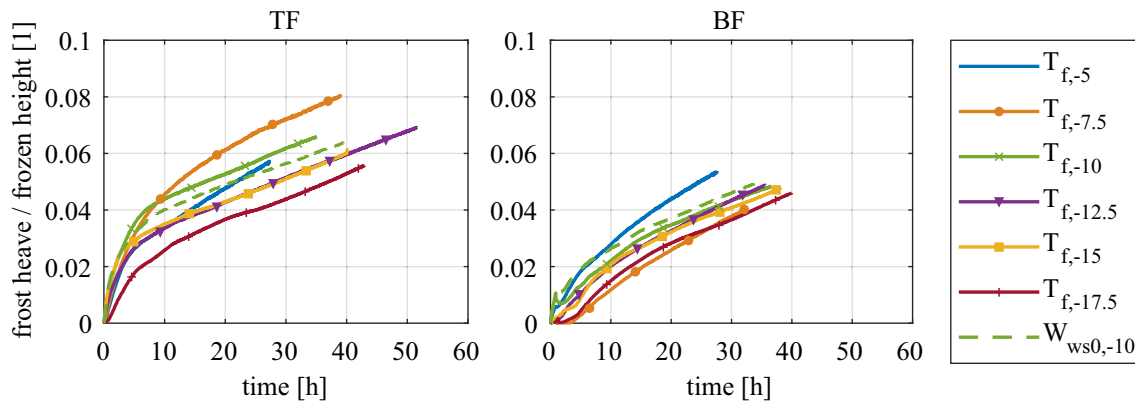


Fig. 10 Frost heave related to the frozen soil part at the thermal transient state for varied absolute freezing temperatures (T_f in $^{\circ}\text{C}$) with (W_{ws0}) and without restricted water supply over time for TF and BF

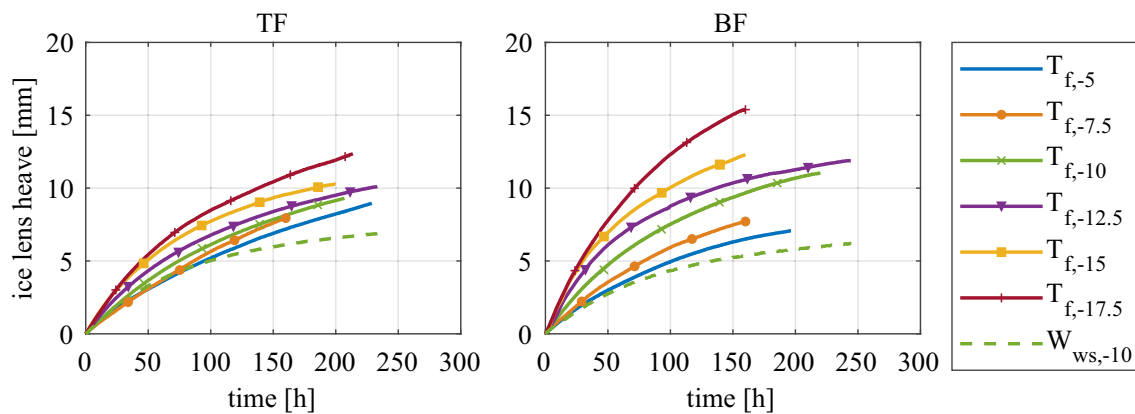


Fig. 11 Ice lens heave at the thermal quasi-steady state for different absolute freezing temperatures (T_f in $^{\circ}\text{C}$) with (W_{ws0}) and without restricted water supply over time for TF and BF

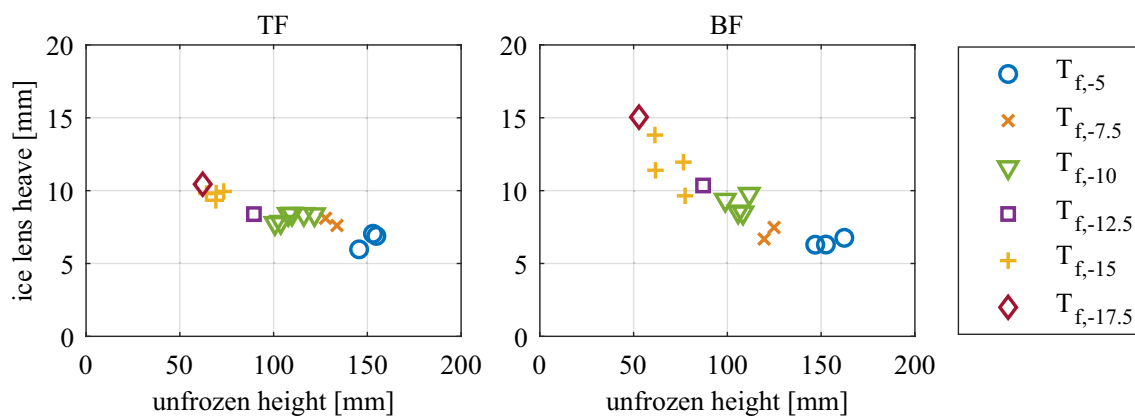


Fig. 12 Ice lens heave for different absolute freezing temperatures (T_f in $^{\circ}\text{C}$) over the height of the unfrozen part after 150 h from the beginning of the quasi-steady state for TF and BF

Figure 12 shows the dependency between frost heave due to ice lens formation and the length of the flow path (unfrozen height) 150 h after the beginning of quasi-steady-

state conditions. With decreasing flow path, ice lens heave increases especially for BF conditions. We explain this difference with TF due to the formation of longitudinal

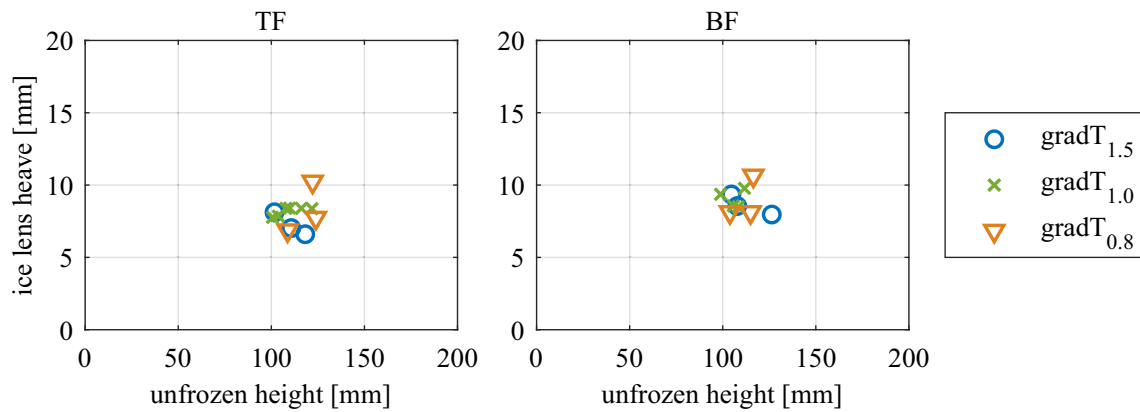


Fig. 13 Ice lens heave for different temperature gradients ($gradT_f$ in $^{\circ}\text{C}/\text{cm}$) along the frozen soil over the height of the unfrozen part after 150 h from the beginning of the quasi-steady state for TF and BF

cracks that facilitate water flow (cf. Fig. 6 in subSect. 3.1) which is exacerbated by the fact that in BF, the water flows downward aided by gravity.

The effect of gravitational water inflow decreases with a thicker unfrozen soil part (i.e., warmer freezing temperatures, T_f) because the cracks do not fully penetrate the unfrozen soil, as shown for temperatures of -5°C and -7.5°C . This explains why for these temperatures, both values in Fig. 12 are very similar for BF and TF. In this case, the heave difference between BF and TF is primarily caused by the overburden load which changes slightly depending on the position of the frost line.

Concluding, the differences on frost heave between TF and BF are attributed to the water flow direction in or against gravity, supported by permeability changes due to cracking. The lower the unfrozen soil height, the greater effect of gravitational water inflow at BF. This can be explained by the hydraulic gradient which increases with decreasing flow path if the hydraulic head and the suction force at the ice lens are the same at each test. This can be assumed because the suction at the ice lens mainly depends

on temperature (e.g., Clausius–Clapeyron equation) and, moreover, the same soil was used for all tests, so the segregation temperature should be the same.

4.2 Temperature gradient $gradT_f$

Figure 13 shows the ice lens heave 150 h after the beginning of the thermal quasi-steady state for temperature gradients of $0.8^{\circ}\text{C}/\text{cm}$, $1.0^{\circ}\text{C}/\text{cm}$ (corresponds to the experiments with $T_f = -10^{\circ}\text{C}$ in subSect. 4.1 due to same freezing depth at thermal quasi-steady state) and $1.5^{\circ}\text{C}/\text{cm}$ along the frozen area. The corresponding heights of the unfrozen area or flow paths are controlled by the temperature boundary conditions. Despite different temperature gradients in the frozen area, the same frost heave occurs. It can be therefore, concluded that the temperature gradient in the frozen area has no relevant impact on the formation of ice lenses at thermal quasi-steady state in the investigated range. This result corresponds to the findings in subSect. 4.1, where the unfrozen height or flow path mainly influences the ice lens heave.

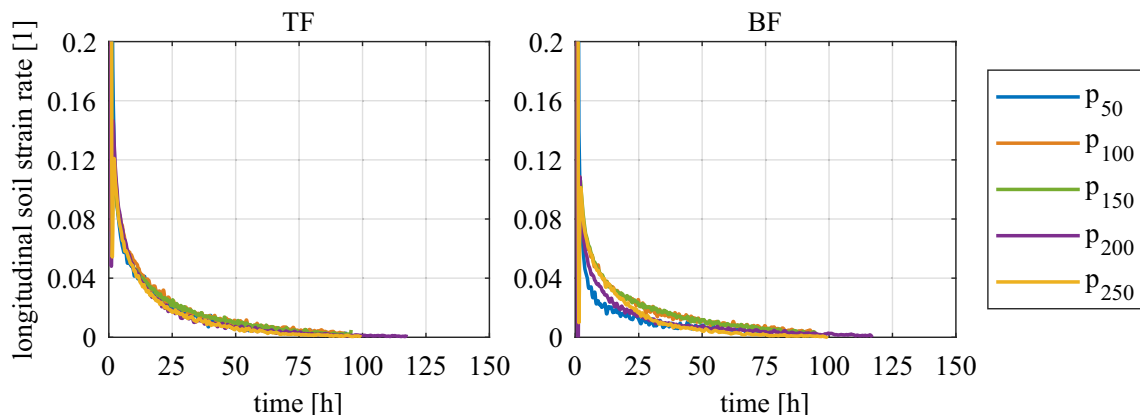


Fig. 14 Longitudinal soil strain during the consolidation phase for different loads (p in kPa) for TF and BF

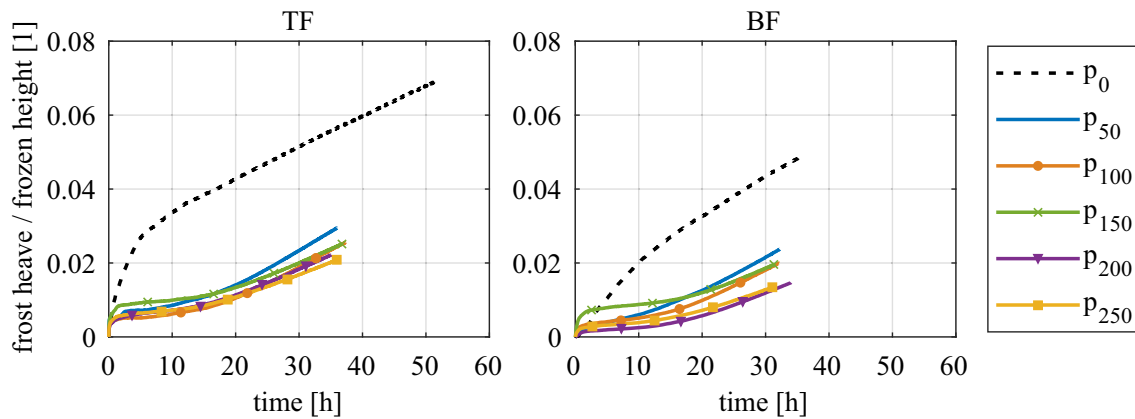


Fig. 15 Frost heave related to the frozen height at the thermal transient state for a freezing temperature of $-12.5\text{ }^{\circ}\text{C}$ and varied loads (p in kPa) for TF and BF

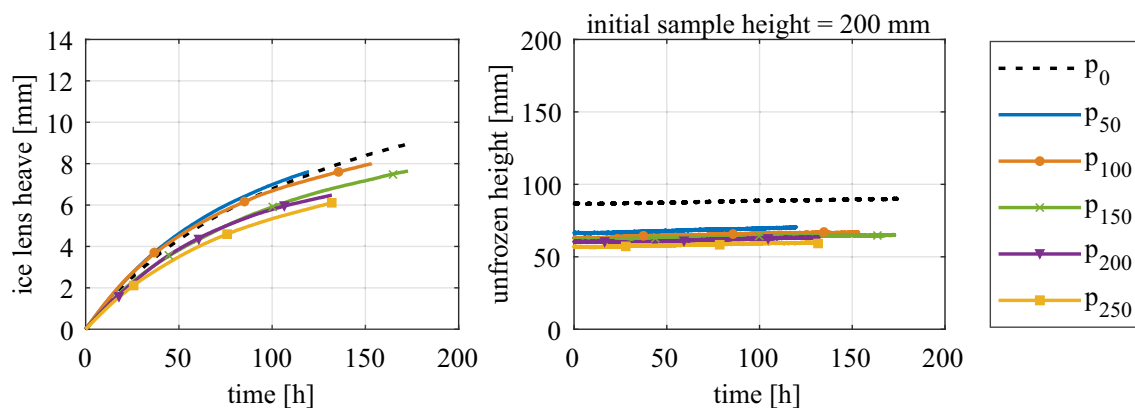


Fig. 16 Ice lens heave (left) and associated unfrozen soil height (right) at the thermal quasi-steady state for a freezing temperature of $-12.5\text{ }^{\circ}\text{C}$ and varied loads (p in kPa) for TF

4.3 External load p

The following tests were carried out by applying a load (p) on the soil sample. Each experiment contains a consolidation and freezing phase. During consolidation phase the soil settles under a defined constant load until the deformation stops. Afterward, the freezing process with a temperature of $-12.5\text{ }^{\circ}\text{C}$ is initiated and frost heaving starts.

Figure 14 shows the longitudinal soil strain rate during consolidation for TF and BF calculated as soil deformation over the maximum settlement at the end of consolidation. After approx. 4 days (96 h) of consolidation, the freezing phase was initiated. The measured settlement fluctuates slightly since the automatic load readjustment just took place every 60 s. The calculation of settlement difference over a time step produces the oscillating curve. At the beginning of the consolidation phase, the specimen is less stiff which increases this effect. To focus the relevant progress over time the ordinate in Fig. 14 ends at 0.2.

During the consolidation phase, the soil settles and water is expelled out of the sample into the external reservoir.

With the beginning of the freezing process, the sample starts to expand due to pore water expansion. Further the emerging suction as a result of thermodynamic unbalance causes the water to flow back into the soil sample and heave due to ice lens formation occurs. The frost heave results during thermal transient freezing are given in Fig. 15 and during thermal quasi-steady state in Fig. 16. For both thermal states, the results are compared with zero load tests p_0 .

The frost heaves during thermal transient freezing (Fig. 15) are related to the height of the frozen part, similar to Fig. 10 (subSect. 4.1), to eliminate influences of the freezing depth on frost heave. The lower porosity resulting from the consolidation phase reduces the frost heave due to pore water expansion compared to zero load freezing. With greater load, frost heave slightly decreases, although the results show the differences between different applied loads are not dramatic. The deviating curve at a load of 150 kN in BF is attributed to irregularities in the initial temperature. Importantly, the formation of a dominating single ice lens at the end of thermal transient freezing, as experienced at zero

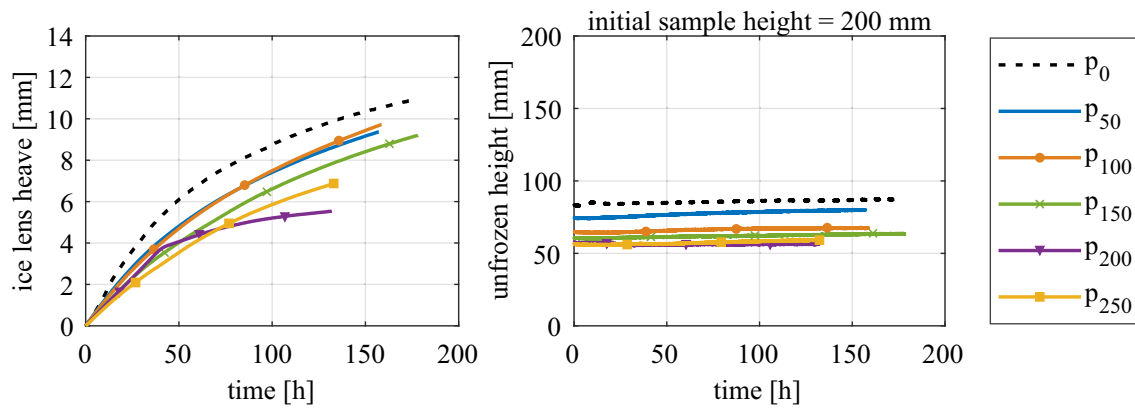


Fig. 17 Ice lens heave (left) and associated unfrozen soil height (right) at the thermal quasi-steady state for a freezing temperature of $-12.5\text{ }^{\circ}\text{C}$ and varied loads (p in kPa) for BF

load tests (cf. Fig. 10), was not observed. Qualitatively there are no differences between the TF and BF results with load, but quantitatively the heave results of TF exceed BF because of less additional soil weight that has to be overcome.

Figures 12 and 13 are shown that the height of the unfrozen area has a great effect on ice lens formation during thermal quasi-steady state. For the examination of ice lens heave during loading, the influence of the unfrozen soil height should be minimized to focus on heave reduction based on the specific load. For this, all tests were carried out with the same freezing temperature of $-12.5\text{ }^{\circ}\text{C}$. However, during consolidation at different load magnitudes changes in porosity and water content occur and influence heat conduction. Thus, the unfrozen heights differ despite of same freezing temperatures (Fig. 16, right, and Fig. 17, right).

Figures 16 and 17 show the ice lens heave as well as the height of the unfrozen soil at the thermal quasi-steady state for a freezing temperature of $-12.5\text{ }^{\circ}\text{C}$ and varied loads. Generally, the frost heave increases with lower loading, but

the results question the influence of the unfrozen height on heaving. For example, comparing BF (Fig. 17) with a load of 50 and 100 kPa the frost heave results are almost similar, but the unfrozen height or flow path for sucked water at 50 kPa is greater. At BF (Fig. 17), the lowest heave value is reached at 200 kPa instead of 250 kPa which could only be explained if the displacement transducer did not work properly in this test. This is because other measured parameters, such as temperature and surcharge are constant when the curve bends.

Besides the effect of unfrozen soil height, the greater difference at BF (Fig. 17) between unloaded and low loaded test results is attributed to the crack formation which influences the sample permeability in the unfrozen area. As expected, greater loading reduces crack formation. (Images are provided in the Supplementary Material 7).

Figure 18 shows, similar to Figs. 12 and 13, the ice lens heave at quasi-steady state conditions for different unfrozen heights 100 h after reaching the thermal quasi-steady state. Since the consolidation phase takes approx. 4 days the freezing phase was selected to 100 h, as 150 h freezing at

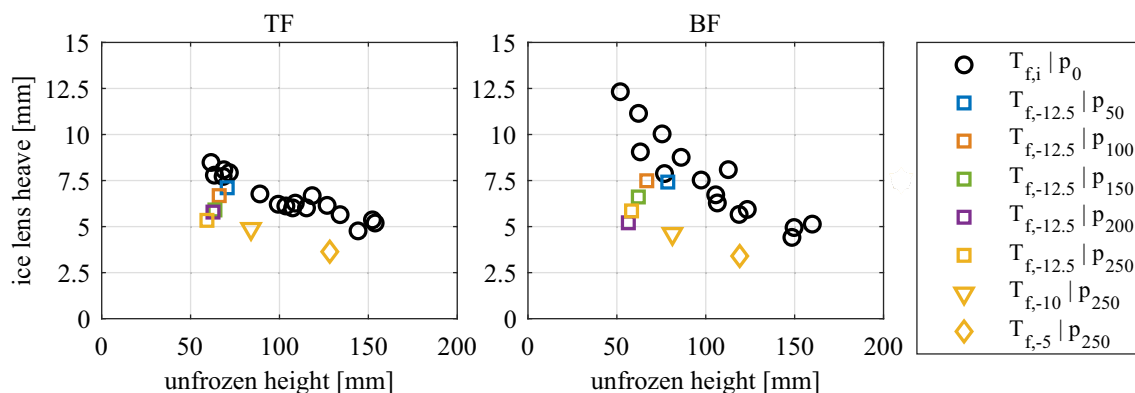


Fig. 18 Ice lens heave at different temperatures (T_f in $^{\circ}\text{C}$) and loads (p in kPa) over the height of the unfrozen part after 100 h from the beginning of the quasi-steady state for TF and BF

thermal quasi-steady-state conditions (cf. Figs. 12 and 13) was not applicable. The black circles indicate the heave results under zero load, carried out in subSect. 4.1.

To investigate the influence of temperature, additional tests using a freezing temperature of $-10\text{ }^{\circ}\text{C}$ and $-5\text{ }^{\circ}\text{C}$ are used for the maximum load of 250 kPa. The ice lens heaving decreases with greater load and, at TF (Fig. 18, left), for 250 kPa is almost parallel to zero load results. At BF (Fig. 18, right), loaded frost heave results are not parallel to the results without loading. It is assumed that the reduced crack formation reduces permeability and therefore the growth of the ice lens. With higher loading TF and BF heaving results are more consistent which emphasize the assumption that the crack-induced increasing permeability and better water accumulation due to gravitational effects at BF is reduced by surcharge.

The results show that besides loading, the influence of the unfrozen soil height or the flow path of sucked water, respectively, is present. The TF and BF results differ as long as the crack formation in the unfrozen area has an effect on the permeability. The greater the magnitude of loading the more crack opening is impeded by confining pressure and the minor heave differences between TF and BF.

5 Conclusion

The method of AGF is common for inner-city tunneling construction projects. Since ice lenses form especially in frost susceptible soils, strong deformations occur, which magnitude depends on the boundary conditions. In this work, the influence of different freezing directions, TF versus BF, on frost heaving, is investigated considering the special thermal and load boundary conditions of an AGF. Therefore, 62 frost heave tests were carried out in a novel test device with testing periods up to 10 days, providing a comprehensive database of ice lens formation during the thermal steady state. This state simulates the holding phase of an AGF, where cooling only maintains the thickness of the frozen body and no further frost penetration occurs.

During the thermal transient phase which is characterized by a growing frost body with moving frost line, there was only a negligible ice lens formation observed which is due to fast frost penetration. The process is dominated by the magnitude of the boundary cold temperatures only. Frost heaving during TF is usually larger than BF heave which is attributed to greater soil weight and consolidation effects in the BF conditions.

At thermal steady state, one relevant factor with great impact on the magnitude of frost heaving is the height of the unfrozen soil, which can also be seen as proxy for the water flow path. This is directly a function of temperature at the boundary conditions where lower temperatures reduce the

unfrozen part (i.e., the colder it is the boundary, the smaller the unfrozen region of the soil). A shorter unfrozen part increases the hydraulic gradient for the same boundary hydraulic conditions and, thus, the water flow velocity to the ice lens. This effect is observed independently of the freezing direction.

Conversely to the transient stage, BF exhibits larger frost heave than TF conditions for almost all conditions. This is due to the formation of longitudinal cracks along the unfrozen zone that initiate during ice lens formation and are caused by suction. The cracks emerge when water at the warm side of the ice lens is drained off for ice lens growth. These cracks favor water flow toward the ice lens, hence, increasing the ice lens size. The closer the ice lens to the water reservoir, the greater is the effect of an improved water accumulation at the growing ice lens. The greatest frost heave occurs when the unfrozen part is short, and cracks reach the unfrozen surface. Equivalent hydraulic conditions can naturally occur in real applications when AGF is used within an aquifer. The application of vertical load reduces crack formation and therefore, for this cases, BF and TF present similar heave magnitudes. In the case of our tests, an applied load of 150 kPa seemed to be the threshold from which the cracks would not form.

The relationship between the unfrozen soil height and the ice lens heave is not linear and different for BF and TF freezing. This is of interest for long-term soil freezing and will be analyzed in detail in future research work.

Supplementary Information The online version contains supplementary material available at <https://doi.org/10.1007/s11440-024-02259-2>.

Acknowledgements This work was supported by the German Research Foundation (DFG) under the project “Investigation and calculation of frost heave considering specific boundary conditions of ground freezing,” grant number 409760547. The funding is herewith gratefully acknowledged.

Author contributions All authors contributed to the study conception and design. Material preparation, data collection and analysis were performed by KN. The first draft of the manuscript was written by KN, and all authors commented on previous versions of the manuscript. All authors read and approved the final manuscript.

Funding Open Access funding enabled and organized by Projekt DEAL.

Data availability The data generated or analyzed during this study are provided within the published article or are available from the corresponding author on reasonable request.

Declarations

Conflict of interest The authors declare there are no competing interests

Open Access This article is licensed under a Creative Commons Attribution 4.0 International License, which permits use, sharing, adaptation, distribution and reproduction in any medium or format, as long as you give appropriate credit to the original author(s) and the source, provide a link to the Creative Commons licence, and indicate if changes were made. The images or other third party material in this article are included in the article's Creative Commons licence, unless indicated otherwise in a credit line to the material. If material is not included in the article's Creative Commons licence and your intended use is not permitted by statutory regulation or exceeds the permitted use, you will need to obtain permission directly from the copyright holder. To view a copy of this licence, visit <http://creativecommons.org/licenses/by/4.0/>.

References

1. Staender W (1967) Das gefrierverfahren im schacht-, grund- und tunnelbau. Die anwendung der kälte in der verfahrens- und klimotechnik, Biologie und Medizin, pp 173–227
2. Hartge KH (1978) Einführung in die bodenphysik. Ferdinand Enke Verlag, Stuttgart
3. Taber S (1929) Frost heaving. *J Geol* 37:428–461
4. Taber S (1930) The mechanics of frost heaving. *J Geol* 38(4):303–317
5. Ruckli R (1944) Die eislinnenbildung im strassenuntergrund. *Schweizerische Bauzeitung* 124(16):206–210
6. Wilen LA, Dash JG (1995) Frost heave dynamics at a single crystal interface. *Phys Rev Lett* 74(25):5076
7. Martin RT (1959) Rhythmic ice banding in soil. *Highway Research Board Bulletin*, p 218
8. Loch JPG (1978) Thermodynamic equilibrium between ice and water in porous media. *Soil Sci* 126(2):77–80
9. Williams PJ, Smith MW (1989) *The frozen earth: fundamentals of geocryology*. Cambridge University Press, Cambridge
10. Unold F (2006) Der Gefriersog bei der Bodenfrostsung und das Kompressionsverhalten des wieder aufgetauten Bodens. Universität der Bundeswehr München, München, Institut für Bodenmechanik und Grundbau
11. Miller R (1972) Freezing and heaving of saturated and unsaturated soils. *Highway Res Rec* 393(1):1–11
12. Konrad J-M, Morgenstern NR (1980) Mechanistic theory of ice lens formation in fine-grained soils. *Can Geotech J* 17(4):473–486
13. Gilpin RR (1980) A model for the prediction of ice lensing and frost heave in soils. *Water Resour Res* 16(5):918–930
14. Nixon JF (1982) Field frost heave predictions using the segregation potential concept. *Can Geotech J* 19(4):526–529
15. O'Neill K, Miller RD (1985) Exploration of a rigid ice model of frost heave. *Water Resour Res* 21(3):281–296
16. Sheng D, Axelsson K, Knutsson S (1995) Frost heave due to ice lens formation in freezing soils: 1. Theory *Verif Hydrol Res* 26(2):125–146
17. Ladanyi B, Andersland O (2004) *Frozen ground engineering*. Wiley
18. Rempel AW (2010) Frost heave. *J Glaciol* 56(200):1122–1128
19. Zhang M, Zhang X, Lai Y, Lu J, Wang C (2020) Variations of the temperatures and volumetric unfrozen water contents of fine-grained soils during a freezing–thawing process. *Acta Geotech* 15:595–601
20. Zhou G, Zou Y, Boley C (2009) Reduktion der Frosthebungen bei der künstlichen Bodenvereisung. *Bautechnik* 86(9):566–573
21. Corte AE (1962) The frost behavior of soils. I. vertical sorting. *Highway Res Board Bull*, p 317
22. Kaplar CW (1970) Phenomenon and mechanism of frost heaving. *Highway Res Rec* 304:1–13
23. Penner E (1957) Soil moisture tension and ice segregation. *Highway Res Board Bull*, p 168
24. Hoekstra P (1969) Water movement and freezing pressures. *Soil Sci Soc Am J* 33(4):512–518
25. Chamberlain EJ (1981) Frost susceptibility of soil. U.S. army corps of engineers—cold regions research and engineering laboratory
26. Dagli D (2017) Laboratory investigations of frost action mechanisms in soils. Department of Civil, Environmental and Natural Resources Engineering, Luleå University of Technology
27. Loch JPG, Kay BD (1978) Water redistribution in partially frozen, saturated silt under several temperature gradients and overburden loads. *Soil Sci Soc Am J* 42:400–406
28. Penner E (1986) Aspects of ice lens growth in soils. *Cold Reg Sci Technol* 13(1):91–100
29. Aitken GW (1974) Reduction of frost heave by surcharge stress. Corps of engineers, US army cold regions research and engineering laboratory
30. Hill D, Morgenstern N (1977) Influence of load and heat extraction on moisture transfer in freezing soils. In: *International symposium on frost action in soils*, Luleå, University of Luleå
31. Chamberlain EJ, Gow AJ (1979) Effect of freezing and thawing on the permeability and structure of soils. *Eng Geol* 13(1–4):73–92
32. Akagawa S (1988) Experimental study of frozen fringe characteristics. *Cold Reg Sci Technol* 15(3):209–223
33. Arenson L, Segó D, Take WA (2007) Measurement of ice lens growth and soil consolidation during frost penetration using particle image velocimetry (PIV). In: *60th Canadian geotechnical conference & 8th joint CGS/IAH-CNC groundwater conference*, Ottawa, Ontario, Canada
34. Arenson LU, Azmarch TF, Segó DC, Biggar KW (2008) A new hypothesis on ice lens formation in frost-susceptible soils. In: *Ninth international conference on permafrost*, Fairbanks, Alaska. 1: 59–64
35. O'Neill K, Miller RD (1982) Numerical solutions for a rigid-ice model of secondary frost heave. US army corps of engineers, cold regions research & engineering laboratory
36. Horne WT (1987) Prediction of frost heave using the segregation potential. Department of Civil Engineering, The University of Alberta, Edmonton, Alberta
37. Nixon JF (1991) Discrete ice lens theory for frost heave in soils. *Can Geotech J* 28(6):843–859
38. Saarelainen S (1992) Modelling frost heaving and frost penetration in soils at some observation sites in Finland: the SSR model. VTT Technical Research Centre of Finland, Tampere University of Technology
39. Fowler AC, Krantz WB (1994) A generalized secondary frost heave model. *SIAM J Appl Math* 54(6):1650–1675
40. Black PB (1995) Rigidice model of secondary frost heave. CRREL report, U.S. Army Cold Regions Research and Engineering Laboratory. 95(12)
41. Talamucci F (2003) Freezing processes in porous media: formation of ice lenses, swelling of the soil. *Math Comput Model* 37(5–6):595–602
42. Kim K, Zhou W, Huang SL (2008) Frost heave predictions of buried chilled gas pipelines with the effect of permafrost. *Cold Reg Sci Technol* 53(3):382–396
43. Style RW, Peppin SS, Cocks AC, Wettlaufer JS (2011) Ice-lens formation and geometrical supercooling in soils and other colloidal materials. *Phys Rev E* 84(4):041402
44. Zhou J, Li D (2012) Numerical analysis of coupled water, heat and stress in saturated freezing soil. *Cold Reg Sci Technol* 72:43–49
45. Sweidan A, Niggemann K, Heider Y, Ziegler M, Markert B (2021) Experimental study and numerical modeling of the thermo-hydro-

- mechanical processes in soil freezing with different frost penetration directions. *Acta Geotech* 17(1):231–255
46. Fu Z, Wu Q, Zhang W, He H, Wang L (2022) Water migration and segregated ice formation in frozen ground: current advances and future perspectives. *Front Earth Sci* 10:826961
 47. Ji Y, Zhou G, Zhou Y, Vandeginste V (2019) Frost heave in freezing soils: a quasi-static model for ice lens growth. *Cold Reg Sci Technol* 158:10–17
 48. Hansson K, Šimůnek J, Mizoguchi M, Lundin LC, Van Genuchten MT (2004) Water flow and heat transport in frozen soil: numerical solution and freeze–thaw applications. *Vadose Zone J* 3(2):693–704
 49. Rempel AW (2007) Formation of ice lenses and frost heave. *J Geophys Res Earth Surf* 112(F2):F02S21. <https://doi.org/10.1029/2006JF000525>
 50. Nishimura S, Gens A, Olivella S, Jardine RJ (2009) THM-coupled finite element analysis of frozen soil: formulation and application. *Géotechnique* 59(3):159–171
 51. Cai H, Hong R, Xu L, Wang C, Rong C (2022) Frost heave and thawing settlement of the ground after using a freeze-sealing pipe-roof method in the construction of the Gongbei Tunnel. *Tunn Undergr Space Technol* 125:104503
 52. Fremond M, Mikkola M (1991) Thermomechanical modelling of freezing soil. In: *International symposium on ground freezing*, p 17–24
 53. Hartikainen J, Mikkola M (1997) General thermomechanical model of freezing soil with numerical applications. In: *Ground freezing 97; frost action in soils*, Balkema, p 101–105
 54. Michalowski RL, Zhu M (2006) Frost heave modelling using porosity rate function. *Int J Numer Anal Meth Geomech* 30(8):703–722
 55. Zhang Y, Michalowski RL (2015) Thermal-hydro-mechanical analysis of frost heave and thaw settlement. *J Geotech Geoenviron Eng* 141(7):04015027
 56. Cai H, Xu L, Yang Y, Li L (2018) Analytical solution and numerical simulation of the liquid nitrogen freezing-temperature field of a single pipe. *AIP Adv* 8(5):055119
 57. Cai H, Liu Z, Li S, Zheng T (2019) Improved analytical prediction of ground frost heave during tunnel construction using artificial ground freezing technique. *Tunn Undergr Space Technol* 92:103050
 58. Niggemann K, Fuentes R (2023) New semi-analytical approach for ice lens heaving during artificial freezing of fine-grained material. *J Rock Mech Geotech Eng* 15(11):2994–3009
 59. Auld FA, Belt J, Allenby D (2015) Application of artificial ground freezing. In: *Proceedings of the XVI ECSMGE*
 60. Johansson T (2009) Artificial ground freezing in clayey soils: laboratory and field studies of deformations during thawing at the bothnia line, KTH
 61. Kaplar CW (1974) Freezing test for evaluating relative frost susceptibility of various soils. US army cold regions research and engineering laboratory
 62. Penner E, Ueda T (1977) The dependence of frost heaving on load application – preliminary results. In: *Proceedings of the international symposium on frost action in soil, Luleå, Sweden*. 1: 92–101
 63. Jin HW, Lee J, Ryu BH, Akagawa S (2019) Simple frost heave testing method using a temperature-controllable cell. *Cold Reg Sci Technol* 157:119–132
 64. Konrad J-M, Morgenstern NR (1981) The segregation potential of a freezing soil. *Can Geotech J* 18(4):482–491
 65. Konrad J-M, Morgenstern NR (1982) Prediction of frost heave in the laboratory during transient freezing. *Can Geotech J* 19(3):250–259
 66. Zhu XF, Wei XY, Huang X, Zhang YP (2013) The formation of ice lenses in unidirectional and multidirectional freezing soil. *Appl Mech Mater* 353:68–73
 67. Lv Z, Xia C, Li Q, Si Z (2019) Empirical frost heave model for saturated rock under uniform and unidirectional freezing conditions. *Rock Mech Rock Eng* 52:955–963
 68. Yang S, Zhang H, Jin H, Hu Y (2023) Influence of freezing directionality on the permeability of silty clay. *Cold Reg Sci Technol* 207:103756
 69. Xia D, Arenson LU, Biggar KW, Sego DC (2005) Freezing process in Devon silt-using time-lapse photography. In: *58th Canadian geotechnical conference, Saskatoon, Saskatchewan*
 70. Mackay JR (1974) Ice-wedge cracks, Garry Island, Northwest Territories. *Can J Earth Sci* 11(10):1366–1383
 71. Niggemann K (2020) Investigation of frost heave considering the boundary conditions of artificial ground freezing. In: *Transportation soil engineering in cold regions*. 2: *Proceedings of TRANSOILCOLD 2019*, Springer Singapore, p 273–283
 72. Yin Q, Andò E, Viggiani G, Sun W (2022) Freezing-induced stiffness and strength anisotropy in freezing clayey soil: theory, numerical modeling, and experimental validation. *Int J Numer Anal Meth Geomech* 46(11):2087–2114

Publisher's Note Springer Nature remains neutral with regard to jurisdictional claims in published maps and institutional affiliations.